TRANSVERSE BEAM PROFILING AND VERTICAL EMITTANCE CONTROL WITH A DOUBLE-SLIT STELLAR INTERFEROMETER*

J. Corbett[†], X. Huang and J. Wu, SLAC National Accelerator Laboratory, Menlo Park, USA
C.L. Li, East China University of Science and Technology, Shanghai, China
T. Mitsuhashi, KEK, Tsukuba, Japan
Y.H. Xu, Donghua University, Shanghai, China
W.J. Zhang, East China University of Science and Technology, Shanghai, China
and the University of Saskatchewan, Saskatoon, Canada

Abstract

Double-slit interferometers are useful tools to measure the transverse the cross-section of relativistic charged particle beams emitting incoherent synchrotron radiation. By rotating the double-slit about the beam propagation axis, the transverse beam profile can be reconstructed including beam tilt at the source. The interferometer can also be used as a sensitive monitor for vertical emittance control. In this paper we outline a simple derivation of the Van Cittert-Zernike theorem, present results for a rotating double-slit measurement and demonstrate application of the interferometer to vertical emittance control using the Robust Conjugate Direction Search (RCDS) optimization algorithm.

INTRODUCTION

The concept of a double-slit visible light SR interferometer for charged-particle beam size measurement was first developed at KEK [1] and has since been widely used at many accelerator facilities [2]. Compared with an optical telescope, the double-slit interferometer has the advantage of removing aperture diffraction effects thereby improving spatial resolution.

Perhaps the most well-known application of the stellar interferometer was Michelson's measurement of the 0.047" angle subtended by α-Orionis [3]. Subsequently the field of stellar interferometry has advanced to include telescope configurations with sophisticated aperture synthesis [4] and non-redundant aperture arrays which have also been applied to measure charged particle beam cross-sections using synchrotron radiation [5].

SPEAR3 has a dedicated SR diagnostic beam line designed to characterize properties of the electron beam. Within the beam line, unfocused visible light travels 16m to an optical bench where it has a rectangular cross-section of 60mm x 100mm. The vertical acceptance of ±3mrad is sufficient to pass almost all of the 500nm wavelength component with measureable edge diffraction around the perimeter of the beam (Fig. 1, inset).

Figure 1 shows a schematic of the beamline including the interferometer optics. At the dipole source point, the electron beam cross-section is approximately 120μm x

20μm depending on the lattice configuration. A stationary ±0.6mrad beam stop at the accelerator midplane protects the Rhodium-coated SR beam extraction mirror from the high heat flux of the primary x-ray beam. Typical interferometer slit separations for horizontal and vertical beam size measurements are 15 mm and 50 mm, respectively [6]. Both the double-slit mask and the CCD camera can be mounted on rotatable stages to enable measurement at arbitrary angles relative to the beam axis.
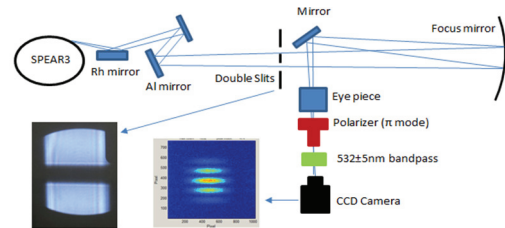
Figure 1: Stellar interferometer on the SPEAR3 visible light diagnostic beam line.

In this paper we first provide a simplified 'conceptual' derivation of the Van Cittert-Zernike theorem to demonstrate the Fourier transform nature of a stellar interferometer operating in the far-field regime. Axial rotation of the interferometer slits about the beam propagation axis is shown to yield the transverse electron beam profile and corresponding beam coherence ellipse in reciprocal space. As an application to machine tuning, vertical interferometer slits are used with a robust optimization program to control vertical beam emittance.

VAN CITTERT-ZERNIKE THEOREM

Analysis of the fringe pattern from a double-slit interferometer in the far field of an incoherent radiating source is often based on the Van Cittert-Zernike theorem [7,8]. In short, the theorem states that under proper paraxial and monochromatic light conditions the fringe contrast evaluated as a function of spatial frequency defined by the slits is the Fourier transform (FT) of the incoherent intensity distribution of the source, $I(x, y)$:

$$\Gamma(f_x, f_y) = \iint I(x, y) e^{-2\pi i (f_x x + f_y y)} dx dy \qquad (1)$$

In practice, by measuring the fringe contrast Γ as a function of slit separation (spatial frequencies f_x, f_y), one can deduce the source profile $I(x, y)$ via the inverse FT.

The application to synchrotron radiation opened the door high-resolution transverse beam profile measurements for charged particle accelerators [1,2]. In this section we present a brief history and a conceptually simple version of the Van Cittert-Zernike theorem that highlights the FT relation.

In the late 19th century A.A. Michelson recognized the double-slit interferometer fringe visibility $\frac{I_{max}-I_{min}}{I_{max}+I_{min}}$ produced from an incoherent source could be used to measure the angular diameter of a star [3]. Later, P.H. Van Cittert calculated partition functions [7], and F. Zernike formalized Michelson's result by integrating over statistically independent radiators in the source and introduced the concept of 'degree of coherence' [8]. This work was re-iterated and expanded by Goodman [9] and Born & Wolf [10] who re-cast the theory in the form of 'Fourier optics', i.e. the source distribution can be represented as a continuous spectrum of plane waves.

Goodman in particular refers to the Van Cittert-Zernike theorem as 'one of the most important theorems of modern optics' and demonstrated the FT nature of the theorem in terms of the propagation of mutual intensity in the far-field.

Born and Wolf stressed time-averaging of the ergodic process in taking the sum over statistically uncorrelated point radiators at the source, and introduced the concept of 'mutual coherence' as the FT of the source intensity in the far-field region. Both developments emphasized that the coherent field component mathematically corresponds to the cross-correlation of the fields evaluated at the two interferometer slits. The derivations hold for rather general conditions and consequently contain intricate mathematical nomenclature.

Here we present simplified steps to illuminate a one-dimensional FT relation between fringe contrast and source profile. Referring to Fig. 2, a classical field $E(y)$ emitted from a single point on the y axis to the left generates an interference pattern with a modulated intensity profile along the y'-axis to the right. The fields arriving at point y' through apertures p_1 and p_2 are

$$E_1(y,y') = \frac{E(y)}{r_1+r_1'}e^{-ik(r_1+r_1')} \qquad (2a)$$

$$E_2(y,y') = \frac{E(y)}{r_2+r_2'}e^{-ik(r_2+r_2')} \qquad (2b)$$

where $E(y)$ statistically fluctuates in amplitude and phase. The light *intensity* at y' is

$$I(y,y') =$$
$$2I(y) + 2Re\{E^*(y)E(y)e^{-ik(r_1-r_2)}e^{-ik(r_1'-r_2')}\} \quad (3)$$

where *I(y)* is the intensity per unit radiator and $Re\{\ \}$ indicates 'real part'. Distance factors are suppressed in the denominator. The cross term on the right is perfectly correlated when fields through slit 1 and 2 originate from the same infinitesimal radiator. The time average of the cross-correlation term is identically zero when the fields originate from different radiators.
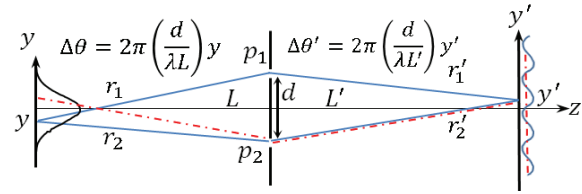
Figure 2: Far-field phase differentials $\Delta\theta = k(r_1 - r_2)$ and $\Delta\theta' = k(r_1' - r_2')$, respectively. Like radiators interfere (blue) and unlike radiators do not interfere (blue and red-dash).

At this point several approximations are typically made prior to integration over the extended source:

a) the intensity pattern is evaluated in the far-field
b) statistically independence (separate points along the y-axis radiate incoherently and do not interfere)
c) quasi-monochromatic light.

Using the far-field approximation, the phase differentials seen in Fig. 2 are [9,10,11]

$$e^{-ik(r_1-r_2)} \sim e^{-2\pi i\left(\frac{d}{\lambda L}\right)y} \qquad (4a)$$

$$e^{-ik(r_1'-r_2')} \sim e^{-2\pi i\left(\frac{d}{\lambda L'}\right)y'} \qquad (4b)$$

Substituting Eq. 4 into 3

$$I(y,y') = 2I(y) + 2Re\left\{E^*(y)E(y)e^{-2\pi i\left(\frac{d}{\lambda L}\right)y}e^{-2\pi i\left(\frac{d}{\lambda L}\right)y'}\right\} \quad (5)$$

Taking the time average over the ensemble of statistically uncorrelated radiators at the source and integrating over source coordinate y gives the total light intensity at observation point y':

$$I(y') = 2I_o\left(1 + Re\left\{\int \frac{I(y)}{I_o}e^{-2\pi i\left(\frac{d}{\lambda L}\right)y}\,dy \cdot e^{-2\pi i\left(\frac{d}{\lambda L'}\right)y'}\right\}\right). \quad (6)$$

with $I(y) = E^*(y)E(y)$ and I_0 is the total intensity at each interferometer slit. The exponential term in the FT 'visibility integral' accounts for the phase shift in the fringe pattern from each independent radiator along the y-axis, $I(y)$. Re-writing in more familiar form

$$I(y',f_y) = 2I_o\big(1 + \gamma(f_y)\cos(2\pi f_y' y')\big) \qquad (7)$$

where $\gamma(f_y) = \frac{1}{I_0}\int I(y)e^{-2\pi i f_y}\,dy$ is the normalized degree of coherence [10], $f_y = \frac{d}{\lambda L}$ is the spatial frequency defined by the slits, and the cosine term produces fringe modulation on the screen. Thus, in the monochromatic far-field approximation, the incoherent source distribution and fringe visibility form a Fourier transform pair with y and f_y the conjugate Fourier transform variables.

DOUBLE SLIT ROTATION

In two dimensions the Van Cittert-Zernike relation can be written

$$\Gamma(f_x, f_y) = \iint I(x, y) e^{-2\pi i (f_x x + f_y y)} dx\, dy \qquad (8)$$

where the configuration-space axes (x,y) and spatial frequencies (f_x, f_y) are referenced to an x-y Cartesian coordinate system. From Eq. 8 a bi-Gaussian beam profile

$$I(x, y) = I_o e^{-\left(\frac{x^2}{2\sigma_x^2} + \frac{y^2}{2\sigma_y^2}\right)} \qquad (9)$$

has a Gaussian degree of coherence function

$$\Gamma(f_x, f_y) = \Gamma_o e^{-\left(\frac{f_x^2}{2\sigma_{\gamma,x}^2} + \frac{f_y^2}{2\sigma_{\gamma,y}^2}\right)} \qquad (10)$$

The expression in the exponent of Eq. 10 indicates the coherence function $\gamma(f_x, f_y)$ is a continuum of concentric ellipses conjugate to the electron beam intensity profile.

Experimentally it is possible to rotate the double-slit system to measure the SR beam coherence as a function of slit observation angle θ. Relative to the x-axis, the projected spatial frequencies become $f_x = \frac{d}{\lambda L} \cos\theta$ and $f_y = \frac{d}{\lambda L} \sin\theta$. For an upright Gaussian beam profile (Eq. 9), the coherence function becomes

$$\Gamma(f_x, f_y, \theta) = \Gamma_o e^{-\left(\frac{\left(\frac{d}{\lambda L}\cos\theta\right)^2}{2\sigma_{\gamma,x}^2} + \frac{\left(\frac{d}{\lambda L}\sin\theta\right)^2}{2\sigma_{\gamma,y}^2}\right)} \qquad (11)$$

To measure angular dependence, a double slit with separation d=16.94 mm was rotated in the unfocused beam from 0 to 180 degrees with a step size of 5 degrees. Figure 3 shows the variation in fringe contrast when the double slit and CCD camera were rotated synchronously around the SR beam axis and the polarizer angle held fixed. In this case the slits were placed in the lower half of the SR beam below the cold finger. The double slit separation distance was a compromise between RMS values for the $\theta = 0°$ and $\theta = 90°$ contrast curves of $\sigma_{\gamma,x} \sim 15$ mm and $\sigma_{\gamma,y} \sim 50$ mm, respectively.

Four data sets corresponding to different values of x-y betatron coupling are plotted in Fig. 3. The displacements in the data along the rotation angle axis correspond to electron beam rotations of θ_0=0°, 9°, 16° and 27°. The theoretical curves according to Eq. 11 are superimposed in the plot. The RMS beam size as measured along the minor axis of the beam ellipse was determined to be σ_{minor}=20, 35, 53 and 69 um.

Figure 4 plots the transverse RMS electron beam profile at the source point with the x-y beam ellipses derived from the fringe contrast data shown in Fig. 3. The electron beam eigen-axes are clearly rotated by coupling of the betafunctions.

BEAM SIZE CONTROL WITH RCDS
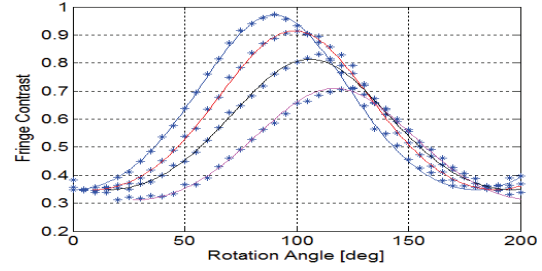
Figure 3: Contrast measured with double-slit rotation for 4 betatron coupling conditions.
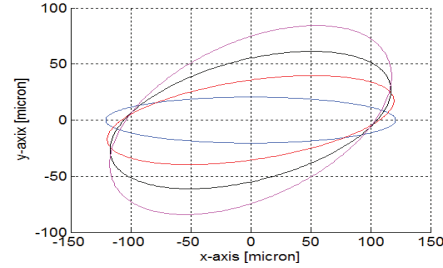
Figure 4: RMS electron beam cross-section color coded for beam coupling conditions in Figure 3.

Optimum accelerator performance frequently requires tuning the magnet lattice with manual or computer-controlled knobs to change machine parameters. In general, accelerator tuning is a multi-variable, nonlinear optimization problem. Most optimization algorithms are not suitable for *online* applications because they are designed to work with smooth mathematical models. Noise in the objective function can cause incorrect steps and hence fail to approach the true optimum.

An algorithm specifically designed for online applications, the *Robust Conjugate Direction Search* (RCDS) [12] overcomes this difficulty. In this section we demonstrate how RCDS was used to control vertical beam size in SPEAR3. Technically, the RCDS algorithm combines the power of Powell's conjugate direction method [12] with a robust, noise-resistant line optimizer. The result is an optimization algorithm for noisy, on-line applications to control multi-variable, non-linear processes.

The RCDS algorithm was initially demonstrated at SPEAR3 by minimizing the betatron coupling using 13 independent skew quadrupoles with the Touschek-dominated beam loss rate as the objective function [12]. Despite the relatively large noise component in the measurements, the algorithm found an optimal solution starting from all skew quadrupole fields set to zero.

For the RCDS applications reported here, the objective function was vertical beam size as measured by the double-slit interferometer. Thirteen skew-quads were again used to control x-y betatron coupling. Referring to Fig. 5, both the interferometer and an x-ray pinhole camera report online values of vertical beam size to the EPICS database. The RCDS algorithm reads these values and performs the

optimization procedure to control the vertical beam size at the interferometer or pinhole camera.
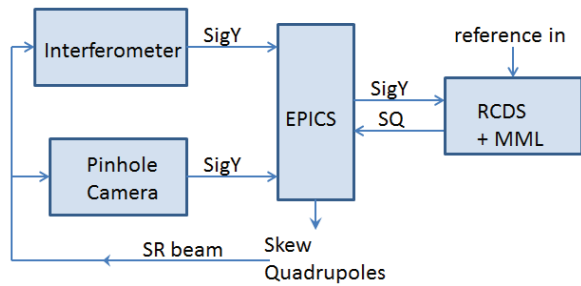
Figure 5: Architecture for RCDS optimization software to control vertical beam size in SPEAR3.
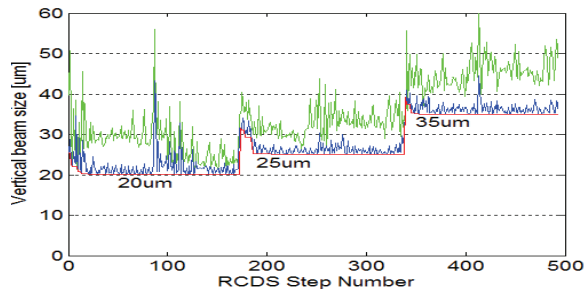
Figure 6: Vertical beam size reference set to 20um, 25um and 30um for the interferometer (blue) and resulting pinhole camera values (red). The two source points have different values for β_y.
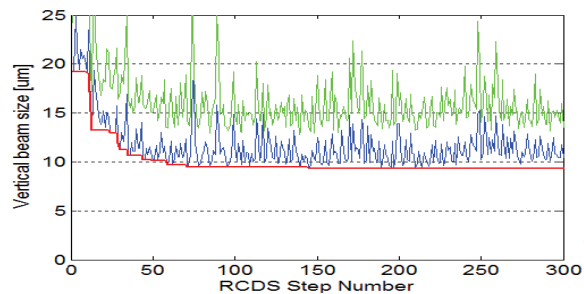
Figure 7: Convergence to minimum vertical beam size with interferometer objective function set to '0'.

The updated skew-quad power supply setpoint values are reported back to EPICS and applied to the lattice magnets.

Figure 6 shows data when the RCDS reference value was set to 20um, 25um and 35um as measured by the interferometer. For each new reference value, the skew quad power supplies were initially set to zero and the algorithm converged within a few minutes. The 'jumps' seen midway along each new search correspond less-than-optimal conditions as the RCDS algorithm explores the phase-space of skew quad eigenvector combinations.

Comparisons were made using the individual skew quads as independent variables against 13 skew quad eigenvector patterns extracted from the Jacobian of the orbit response matrix with respect to each skew quad setting. For each run the eigenvector method converged more quickly because the eigenvectors are inherently more orthogonal than the individual skew quad supplies.

Figure 7 shows the case where the RCDS reference was set to zero (minimum coupling). The red line underlying the data indicates conditions with minimum objective function value. Application of the corresponding skew quad power supply settings produced a minimum value of σ_y=9.5um as measured at the interferometer. Further tests using electron beam Touschek lifetime are planned to determine whether σ_y=9.5um is the minimum resolution limit of the interferometer or the minimum achievable coupling value with only 13 skew quadrupoles.

CONCLUSION

In this paper we report on application of a double-slit interferometer in use at SPEAR3 A simplified derivation of the Van Cittert-Zernike theorem is provided to demonstrate the origin of the Fourier transform relation between incoherent source distribution and fringe contrast evaluated as a function of spatial frequency. Rotation of the double-slit system with respect to the beam axis yields a modulates the fringe visibility and can be used as a tomographic 'slicing' tool to extract the x-y beam intensity profile in agreement with theory. The interferometer was then applied as a measurement tool to control vertical electron beam size using the Robust Conjugate Directional Search algorithm (RCDS).

ACKNOWLEDGMENTS

REFERENCES

[1] T.M. Mitsuhashi, 'Beam Profile and Size Measurements by SR Interferometers,' in Beam Measurements, Joint US-CERN-Japan-Russia School, Montreaux, Switzerland, World Scientific (1998).

[2] T.M. Mitsuhashi, "Recent Trends in Beam Size Measurements Using Spatial Coherence of Visible Synchrotron Radiation", *IPAC15*, Richmond, VA, USA (2015), paper THYC2.

[3] A.A. Michelson and F.G. Pease, "Measurement of the Diameter of α-Orionis with the Interferometer", *Astrophysical Journal*, 249-258 (1921).

[4] A. Labeyrie, *et al.*, "An Introduction to Optical Stellar Interferometry", *Cambridge University Press* (2006).

[5] P. Skopintsev, *et al.*, "Characterization of spatial-coherence of synchrotron radiation with Non-Redundant Arrays of Apertures", JSR 21 (2014).

[6] C.L. Li, et al, "Double-slit Interferometer Measurements at SPEAR3', *IPAC16* (2016), paper MOPMR054.

[7] P.H. Van-Cittert, Physica 1, 2001 (1934).

[8] F. Zernike, 'The Concept of Degree of Coherence and Application to Optical Problems', Physica, 5 (1938).

[9] J. Goodman, 'Statistical Optics', Wiley & Sons (1985).

[10] M. Born and E. Wolf, "Principles of Optics", Sixth Edition, Pergamon Press (1980).

[11] J. Peatross and M.Ware, "Physics of Light and Optics," Brigham Young University, unpublished, (2008).

[12] X. Huang, *et al.*, "An Algorithm for Online Optimization of Accelerators", NIM A 726 77-83 (2013), and references therein.